SANDIA REPORT

SAND88–2693 • UC–32
Unlimited Release
Printed May 1989

Cavity Dimensions for High Velocity Penetration Events – A Comparison of Calculational Results With Data

Lubomyra N. Kmetyk, Paul Yarrington

Prepared by
Sandia National Laboratories
Albuquerque, New Mexico 87185 and Livermore, California 94550
for the United States Department of Energy
under Contract DE-AC04-76DP00789

When printing a copy of any digitized SAND Report, you are required to update the markings to current standards.

Issued by Sandia National Laboratories, operated for the United States Department of Energy by Sandia Corporation.

NOTICE: This report was prepared as an account of work sponsored by an agency of the United States Government. Neither the United States Government nor any agency thereof, nor any of their employees, nor any of their contractors, subcontractors, or their employees, makes any warranty, express or implied, or assumes any legal liability or responsibility for the accuracy, completeness, or usefulness of any information, apparatus, product or process disclosed, or represents that its use would not infringe privately owned rights. Reference herein to any specific commercial product, process, or service by trade name, trademark, manufacturer, or otherwise, does not necessarily constitute or imply its endorsement, recommendation, or favoring by the United States Government, any agency thereof or any of their contractors or subcontractors. The views and opinions expressed herein do not necessarily state or reflect those of the United States Government, any agency thereof or any of their contractors.

Printed in the United States of America. This report has been reproduced directly from the best available copy.

Available to DOE and DOE contractors from
Office of Scientific and Technical Information
PO Box 62
Oak Ridge, TN 37831

Prices available from (615) 576-8401, FTS 626-8401

Available to the public from
National Technical Information Service
US Department of Commerce
5285 Port Royal Rd
Springfield, VA 22161

NTIS price codes
Printed copy: A03
Microfiche copy: A01

Distribution
Category UC-32

SAND88-2693
Unlimited Distribution
Printed May 1989

Cavity Dimensions for High Velocity Penetration Events - A Comparison of Calculational Results with Data

Lubomyra N. Kmetyk
Computational Physics & Mechanics Division I
and
Paul Yarrington
Computational Physics & Mechanics Division II
Sandia National Laboratories
Albuquerque, New Mexico

ABSTRACT

Calculations were performed with the CTH and HULL finite difference wavecodes to evaluate computational capabilities for predicting depth and diameter of target cavities produced in high velocity penetration events. The calculations simulated selected tests in a set of armor penetration experiments conducted by the U.S. Army Ballistic Research Laboratory and reported earlier in the literature. The tests and simulations involved penetration of semi-infinite targets by long rod projectiles over a range of impact velocities from 1.3 to 4.5 km/sec. Comparisons are made between the calculated and measured dimensions of the target cavities, and the sensitivity of the predicted results to target property variations is investigated.

Contents

1 Introduction **2**

2 Description of Problem **3**

3 Description of Calculations **4**

3.1 CTH Calculations 4

3.1.1 CTH Code Features 4

3.1.2 CTH Computational Model 4

3.2 HULL Calculations 5

3.2.1 HULL Code Features 5

3.2.2 HULL Computational Model 5

4 Description of Results **7**

4.1 CTH Results 7

4.1.1 Baseline Calculations 7

4.1.2 Zoning Study 7

4.1.3 RHA Yield Strength Study 8

4.2 HULL Results 8

4.2.1 Baseline Calculations 8

4.2.2 Sensitivity Studies 9

5 Discussion and Conclusions **10**

APPENDIX A. CTH Calculations **32**

A.1 CTH Input Deck 32

A.2 CTH Code Version 32

A.3 CTH Output Files 32

APPENDIX B. HULL Calculations **35**

B.1 HULL Input Deck 35

B.2 HULL Code Version 35

B.3 HULL Output Files 35

1 Introduction

In analyses of high-velocity penetration problems, prediction of penetration depth has traditionally been the subject of most interest. A number of recent applications of penetrator technology, however, have focused attention on the accuracy of analytical techniques for predicting the diameter, as well as the depth, of the target cavity. Although little information is available on time-dependent, radial growth of the target cavity in penetration events, data on final cavity dimensions are available for checking the analytical results. Favorable comparison between measured and calculated *final* cavity diameter gives some measure of confidence in our ability to predict hole growth dynamics during these events.

This report discusses calculations done with the CTH [1] and HULL [2] finite difference wavecodes to predict cavity depth and diameter in high-velocity penetration events. The calculations simulated selected tests from a series of armor penetration experiments conducted earlier by Silsby [3] of the U.S. Army Ballistic Research Laboratory, and comparisons are shown between the calculated and measured final cavity dimensions.

The computer codes and models used for the calculations are described in Section 2, while Section 3 presents the calculational results and shows comparisons with the data. A discussion of the results and the conclusions of the study are presented in Section 4. The appendices list input decks and provide information on code versions/modifications used for the calculations. Information is also provided on file storage for the calculational results on the SNLA central computing system.

2 Description of Problem

The calculations described here model penetration of semi-infinite steel target blocks by tungsten alloy, long rod projectiles, where the impact velocity ranged from 1.3 to 4.5 km/sec. The projectiles had a length-to-diameter ratio (L/D) of 23 and were of two different scales, corresponding to masses of 50 and 100gm. Table 1 lists the entire set of test conditions as reported in Reference [3]. The present study simulated selected tests from this set, as discussed in Section 4, below.

Material properties for the projectiles were chosen to model the Kennametal tungsten alloy, W10 [4], while material properties appropriate for thick plates of rolled homogeneous armor (RHA) were used for the steel target blocks. The majority of the calculations were done with a baseline set of "best-estimate" properties for the penetrator and target materials; however, additional calculations were done to investigate the effect of material property variations on the predicted results. The material properties used in the calculations can be found in the CTH and HULL input listings in the appendices to this report and are discussed further in Section 4, below.

3 Description of Calculations

3.1 CTH Calculations

3.1.1 CTH Code Features

The CTH code [1] was developed to model a wide range of solid dynamics problems involving shock wave propagation and material motion in one, two or three dimensions. The finite-difference analogs of the Lagrangian equations of momentum and energy conservation are employed with continuous rezoning to construct Eulerian differencing. CTH has equation-of-state models suitable for most conditions encountered in shock physics. Models are also included for treating material strength and fracture and for treating distended (porous) materials and high explosives.

3.1.2 CTH Computational Model

The CTH calculations were done using two-dimensional, axisymmetric coordinates, with the target modeled as a semi-infinite body, i.e., infinite in depth and lateral extent. The zoning used in the *baseline* CTH calculations employed non-square cells in the penetrator/target interaction region, primarily because of the large L/D of the rod. In the radial direction, the mesh started at the symmetry axis and used 50 cells of width 0.1cm, followed by an additional 10 cells of uniformly increasing size (at a 2.5% rate) to an outer radius of ~10cm. In the axial direction, the initial mesh included 250 cells of length 0.2cm, which covered the penetrator and extended 20cm into the target. An additional 50 cells of uniformly increasing size (at a 5% rate) were used to model the target to a depth of ~70cm. For the two projectile sizes considered here, this zoning provided 2-4 cells across the radius of the rods and 60-80 cells along their length. Transmitting boundary conditions were used at the outer radial and axial edges of the mesh.

An additional, more finely-zoned calculation was done to investigate zoning sensitivity. For this case, the size of the cells in the central "subgrid" was reduced by a factor of two in each direction. This resulted in a subgrid of 100x500 cells, with the cell size being 0.05cm in the radial direction and 0.10cm in the axial direction. As before, additional cells of uniformly increasing size were used in both directions to model outer regions of the target.

The iron and tungsten equations-of-state available in the ANEOS [5] library were used for the projectile and target materials, respectively. The input deck for a typical

CTH baseline calculation is listed in Appendix A. Material property constants are included in the input listing found in the appendix and are discussed in more detail in Section 4, below.

3.2 HULL Calculations

3.2.1 HULL Code Features

The HULL code system [2] consists of a set of computer programs for generating and solving continuum dynamics problems, plus assorted peripheral programs to process and display the results of the calculations. As currently configured, HULL solves two- and three-dimensional Eulerian and Lagrangian problems, and provides various means for linking the two types of solutions. Virtually all material property data are read from an extensive material library file, MATLIB, which specifies the equation-of-state and strength formulation for the material, as well as default values for the material properties. Most of the solids in HULL (including those relevant to the present problem) utilize the Mie-Gruneisen equation-of-state in the code.

3.2.2 HULL Computational Model

The HULL calculations were done in the Eulerian mode, using two-dimensional axisymmetric coordinates. In all but one of the HULL calculations, the target was treated as semi-infinite. The computational mesh for the *baseline* HULL calculations employed a constant subgrid of 10x500 nonsquare cells. In the radial direction, the mesh started at the symmetry axis and used 10 cells of width 0.05cm, followed by 190 additional cells of uniformly increasing size (at 5% rate). In the axial direction, the mesh used 500 cells of length 0.1cm, extending 16cm into the air (i.e., just beyond the back end of the penetrator at the time of impact) and 34cm into the target. An additional 50 cells of uniformly increasing size (at a 10% rate) were used in the target to a depth of ~160cm. For the two projectile sizes considered here, this zoning provided 5-8 cells across the radius of the rods and 100-160 cells along their length.

(Note that the baseline HULL model is essentially equivalent to the CTH fine-zone model. The primary reason that the baseline zonings for the two codes, chosen to yield similar computational accuracy, differ by a factor of two is the availability of an advanced, second order convection scheme [6] in CTH.)

The RHA target was modeled in the baseline calculations using the "ssteel" material properties from the HULL material library, MATLIB, with material strength constants modified to be consistent with the material properties listed in Table 1. Likewise, to treat the alloy used for the projectiles in the tests simulated here, the default MATLIB constants for tungsten were modified to correspond to the values in Table 1. These

"best-estimate" material property constants for the HULL baseline calculations are included in the input listing provided in the Appendix and are discussed in more detail in Section 4. All of the baseline calculations used these same material properties.

4 Description of Results

In the comparisons below, the hole diameter is normalized by the effective penetrator diameter (D_E), and the hole depth is normalized by the penetrator length. In the penetration tests [3], the projectiles were threaded over much of their length, and D_E was defined to be the diameter of a uniform cylinder having the same length and total volume as the actual, threaded, hemispherically-nosed penetrator. For the calculations, the projectiles were assumed to be straight-sided rods of diameter D_E.

Following the penetration tests, the target blocks were sectioned along the length of the cavity channel, and the cavity diameter, as reported in [3], was measured "a short distance below the surface [7]". Figure 1, from [8], shows the cavity profile for one of the 4.4 km/sec impact tests. In general, the cavity wall was found to be relatively rough, and a narrowing of the channel was observed in many of the tests at the struck surface. These features were also observed in the calculational results discussed below. The cavity dimensions in all the calculations were determined from material interface contours produced by the graphics program. The interface lines represent material volume fraction contours separating computational cell regions that are less than half full of target material from regions that are more than half full of target material.

4.1 CTH Results

4.1.1 Baseline Calculations

Table 2 lists the baseline CTH calculations that were performed in this study and compares the calculated results for cavity diameter and depth with the test data. As indicated, two penetrator scales (50gm and 100gm) were modeled, and four calculations were done for each scale to span the velocity range of interest.

Figures 2-5 show cavity profiles at an early time and a late time in the event for each of the 100gm rod calculations. Plots comparing the measured and calculated results for cavity diameter and depth are shown in Figures 6 and 7, respectively. It should be noted that the predicted cavity shape is not perfectly cylindrical, but has "bulges" along its length. Thus, a range of values is reported in Table 2 and shown in Figure 6 for the calculated cavity diameter, corresponding to the maximum and minimum diameter along the penetration path. It should also be noted that, as was observed in the test program, the lowest velocity event shows the rod being decelerated to a stop, with a length of uneroded penetrator material remaining in the target. In the majority of the calculations, however, the entire rod is consumed, as was observed in the tests.

4.1.2 Zoning Study

As mentioned in Section 2.1.2, one calculation (viz., a 100gm rod with an impact velocity of 4.4km/s) was rerun with the zoning resolution increased by a factor of two

to evaluate sensitivity of the calculated results to zoning. Figure 8 compares the cavity shape for the two calculations. The maximum cavity diameter is slightly larger (viz., 3.62 vs 3.46cm) and slightly deeper (viz., 24.6 vs 24.4cm) for the more finely-zoned calculation than for the baseline case. Thus, increasing the resolution by a factor of two has less than a 5% effect on the calculated results. From this we would conclude that the baseline zoning (as described in Section 2.1.2) is entirely adequate.

4.1.3 RHA Yield Strength Study

Reference [9] indicates that an appropriate value of yield strength for steels of the hardness levels indicated in Table 1, i.e., BHN 230-270, is in the range of 7.5-9.0kbars. For the baseline CTH calculations, we chose a value of 7.5kbar for the yield strength of the target material, while the fracture strength was set to 20kbar. To assess the effect of material strength on the calculations, sensitivity studies were performed in which the yield strength was varied from 5 to 15kbar. The case of a 100gm rod with an impact velocity of 4.4km/s was modeled for those calculations. The results for cavity diameter and depth are shown in Figures 9 and 10, respectively. While the predicted cavity depth appears to be relatively insensitive to these changes in the target strength, the predicted cavity diameter shows a very strong dependence on the strength properties assumed for the target. Figure 11 shows the effect on the predicted cavity geometry of doubling the target yield strength from 7.5 to 15kbar.

4.2 HULL Results

4.2.1 Baseline Calculations

Table 3 lists the baseline HULL calculations and compares the predicted cavity diameter and depth with the test data. The calculational set included only events involving the larger scale (i.e., 100gm) penetrators, and corresponded to the same impact conditions for that penetrator size as were simulated with CTH.

Figures 12-15 show cavity profiles for the HULL calculations, and plots comparing predicted and measured values for cavity diameter and depth are shown in Figures 16 and 17, respectively. Notice, again, that the predicted cavity shape has "bulges" along its length, and the range reported for cavity diameter corresponds to the maximum and minimum values along the penetration path. From Figure 12 it can be seen that, in the HULL calculations, as was observed in the CTH results and in the test program, a portion of uneroded penetrator remains in the bottom of the cavity in the lowest velocity event.

(Note that both CTH and HULL give similar results with baseline computational models whose cell size differs by a factor of two in code dimension. As a result, the total problem size differs by four and the total run times differ by eight. The improved

efficiency of CTH is primarily due to its advanced second order convection scheme as noted in Section 3.2.2.)

4.2.2 Sensitivity Studies

The RHA target was modeled in the baseline calculations using the default "ssteel" material properties from the HULL material library, MATLIB, with the yield strength set to 7.5kbar to be consistent with Reference [9], as noted in Section 4.1.3, above. In order to evaluate the influence of material strength on the cavity predictions, a few additional calculations were done using a 15kbar yield strength, typical of harder, thin plates of RHA. A calculation was also done in which the "rupture strain" was reduced from 30% to 15%, to assess the effect of the material failure modeling on the predicted results.

The qualitative behavior seen in the test data is correctly reproduced by the HULL calculations, as noted above, and the quantitative agreement was found to be much better when the lower yield strength (7.5kbar) was used for the target than when the higher (15kbar) yield strength was used. Figure 18 shows the effect on cavity geometry of increasing the target yield strength from 7.5 to 15kbar, for the problem of a 100gm rod with an impact velocity of 4.4km/s. In the high strength calculations the hole diameters were significantly smaller than were measured in the tests, except at the lowest impact velocities, with the discrepancy increasing as the penetrator velocity was increased. Reducing the rupture strain, as indicated above, had no significant effect on the predicted cavity dimensions.

5 Discussion and Conclusions

The comparisons shown in this study between calculational results and experimental values for cavity dimensions in high velocity penetration events are quite encouraging. Depth of penetration was predicted within a few percent of the test results in all cases, while cavity diameter predictions were seen to be in good qualitative agreement (within ~25%) with the test data. Furthermore the *trend* in cavity depth and diameter with increasing projectile velocity was predicted well.

It is interesting to note how much more accurately the codes are able to predict the cavity depth than its diameter. This is likely due to the fact that our material models are less accurate in the low stress regime where material strength effects are important. Much of the radial growth of the cavity occurs at late-time in the event, when stresses would be in this strength-dominated regime, where the material modeling is less accurate. On the other hand, during penetration, pressures ahead of the projectile are well above the shear strength of either of the materials, and the codes are better able to model the penetration and erosion processes in that regime.

It should be noted, however, that the penetration process is not strictly hydrodynamic. In particular, the cavity depth is strongly dependent on the projectile impact velocity, which is contrary to a hydrodynamic theory of penetration.

Finally, since much of the radial cavity growth occurs in the low stress regime, when strength effects are important, it is not surprising that the calculated cavity diameter was quite sensitive to the material strength assumed for the target. The results emphasize, however, that if cavity diameter is an important issue in a calculational study of ordnance velocity penetration, it is imperative to use realistic models and appropriate material properties for the target shear strength.

Bibliography

[1] McGlaun, J. Michael, S. L. Thompson and M. G. Elrick, "CTH User's Manual and Input Instructions", SAND88-0523, Sandia National Laboratories, Albuquerque, NM, 4/88.

[2] Matuska, Daniel A. and John J. Osborn, "HULL Documentation Volume I: Technical Discussion; Volume II: Users Manual", Orlando Technology, Inc., Shalimar, Florida, 10/87.

[3] Silsby, Graham F. "Penetration of Semi-Infinite Steel Targets by Tungsten Long Rods at 1.3 to 4.5 km/s", Proceedings ADPA Eighth International Symposium on Ballistics, Orlando, Florida, 10/84.

[4] Trademark, Kennametal Inc., Latrobe, Pa.

[5] Thompson, S. L. and H. S. Lauson, "Improvements in the Chart-D Radiation-Hydrodynamic Code III: Revised Analytic Equations of State", SC-RR-71 0714, 3/72 (Reprinted 2/84).

[6] McGlaun, J. Michael, "Improvements in CSQII: An Improved Numerical Convection Algorithm", SAND82-0051, Sandia National Laboratories, Albuquerque, NM, 1/82.

[7] Graham F. Silsby, private communication.

[8] Data Package: BRL KE Penetrator Impact Test, USAF Arnold Engineering Development Center, Project Engineer: J. R. Blanks, Test Period: 7/25/83 - 8/3/83.

[9] Metals Handbook, Volume 1, Properties and Selection of Metals, American Society for Metals, 8th Edition, 1961, p1234.

Table 1. Test Conditions

Penetrator:	
Material	W10 (sintered 90W-7Ni-3Fe alloy)
Density	17.3 gm/cc
Hardness	Rockwell C 40.6
Tensile Properties	169 ksi yield strength at 0.2% offset
	172 ksi ultimate strength
	10.6% elongation to rupture
Compressive Properties	174 ksi yield strength at 0.2% offset
	191 ksi yield strength at 1.0% offset
Target:	
Material	6-8in thick RHA
Surface Hardness	Brinnel 270.4 (6in)
	Brinnel 231.6 (8in)

	Penetrator			Cavity	
Test ID	Length (cm)	D_E (cm)	Velocity (km/s)	Depth (cm)	Diameter (cm)
R12 1929	15.578	0.687	1.291	8.0	1.25
R12 1928	15.583	0.682	1.494	11.2	1.20
VKG 5833	15.583	0.683	1.865	17.45	1.40
VKG 5841	12.179	0.528	2.365	16.52	1.30
VKG 5840	12.179	0.535	2.409	17.23	1.32
VKG 5835	15.583	0.676	2.653	22.85	1.92
VKG 5834	15.583	0.670	2.742	22.80	1.87
VKG 5843	12.179	0.515	2.746	17.63	1.50
VKG 5838	15.583	0.680	3.335	23.79	2.45
VKG 5839	15.583	0.528	3.449	24.15	2.60
VKG 5842	12.179	0.527	3.580	18.86	2.01
VKG 5837	15.575	0.669	4.398	24.69	3.49
VKG 5836	15.583	0.686	4.415	24.81	3.60
VKG 5844	12.169	0.524	4.525	19.37	2.72

Table 2. CTH Baseline Calculational Results - Comparison with Data

(100 gm Projectiles)

Test ID	Velocity[1] (km/s)	Cavity Diameter[2] Calculation (cm)	Cavity Diameter[2] Test Data (cm)	Cavity Depth Calculation (cm)	Cavity Depth Test Data (cm)
R12 1928	1.5	1.08-1.38	1.20[3]	12.1	11.20
VKG 5835	2.7	1.77-2.15	1.886-2.170	22.3	22.85
VKG 5838	3.3	2.15-2.54	2.305-2.625	24.4	23.79
VKG 5837	4.4	2.62-3.46	3.385-3.680	24.4	24.69

(50 gm Projectiles)

Test ID	Velocity[1] (km/s)	Cavity Diameter[2] Calculation (cm)	Cavity Diameter[2] Test Data (cm)	Cavity Depth Calculation (cm)	Cavity Depth Test Data (cm)
VKG 5841	2.3	1.23-1.54	1.220-1.526	17.5	16.52
VKG 5843	2.7	1.31-1.69	1.349-1.658	17.3	17.63
VKG 5842	3.6	1.54-2.15	1.924-2.192	18.8	18.86
VKG 5844	4.5	2.08-2.77	2.447-2.735	19.7	19.37

Table 3. HULL Baseline Calculational Results - Comparison with Data

(100 gm Projectiles)

Test ID	Velocity[1] (km/s)	Cavity Diameter[2] Calculation (cm)	Cavity Diameter[2] Test Data (cm)	Cavity Depth Calculation (cm)	Cavity Depth Test Data (cm)
R12 1928	1.5	1.00-1.30	1.20[3]	10.51	11.20
VKG 5835	2.7	1.60-2.01	1.886-2.170	21.2	22.85
VKG 5838	3.3	2.02-2.41	2.305-2.625	22.5	23.79
VKG 5837	4.4	2.61-3.23	3.385-3.680	23.6	24.69

[1] Nominal

[2] The range of values reported here corresponds to variations in diameter observed along the cavity to a depth of 5-6 projectile diameters below the surface.

[3] Cavity profile was not available in Reference [8]; value reported is that given in Reference [3].

Figure 1. Sectioned View [8] of Cavity for Test
at Impact Velocity of 4.4 km/sec

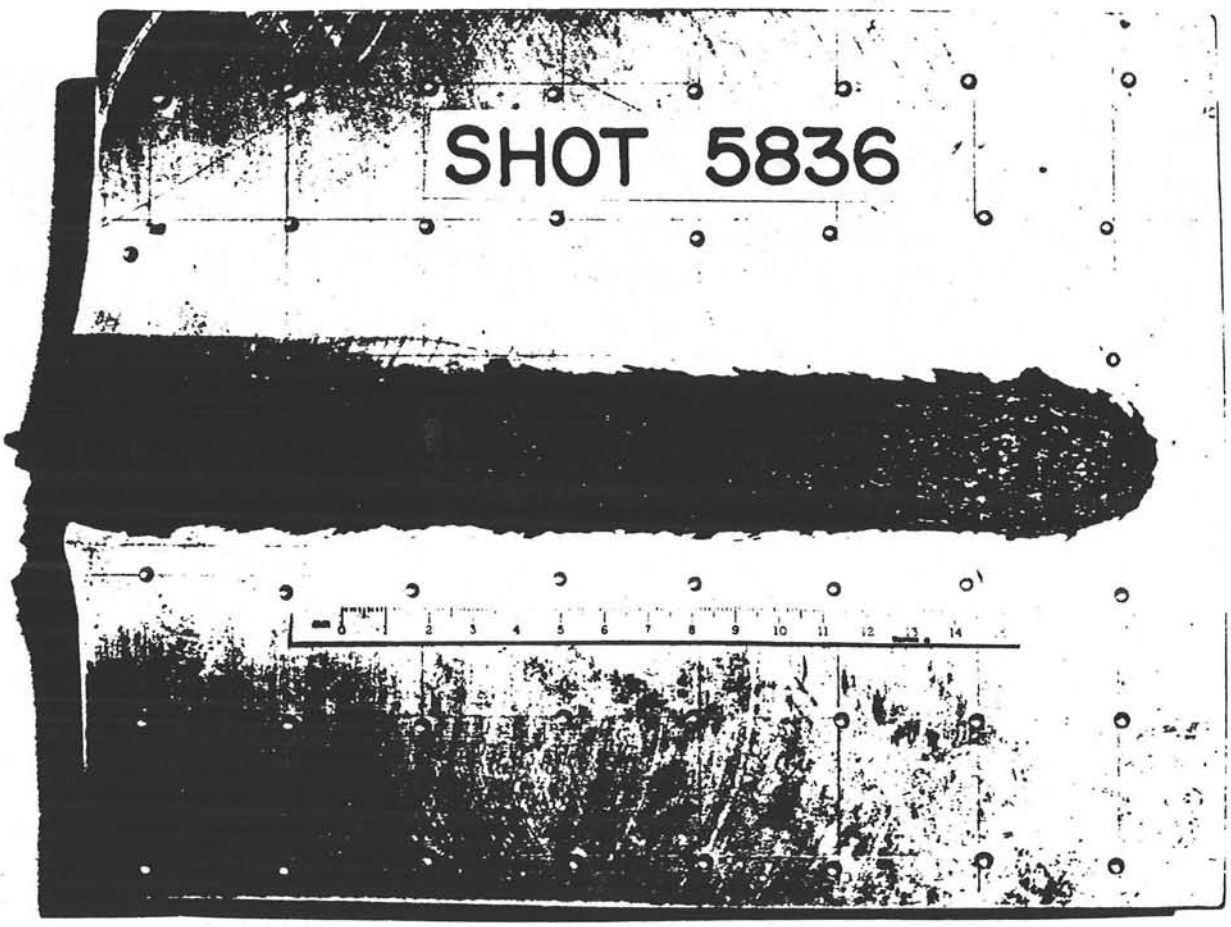

Figure 2. CTH Calculational Results for 1.5km/sec Impact Velocity

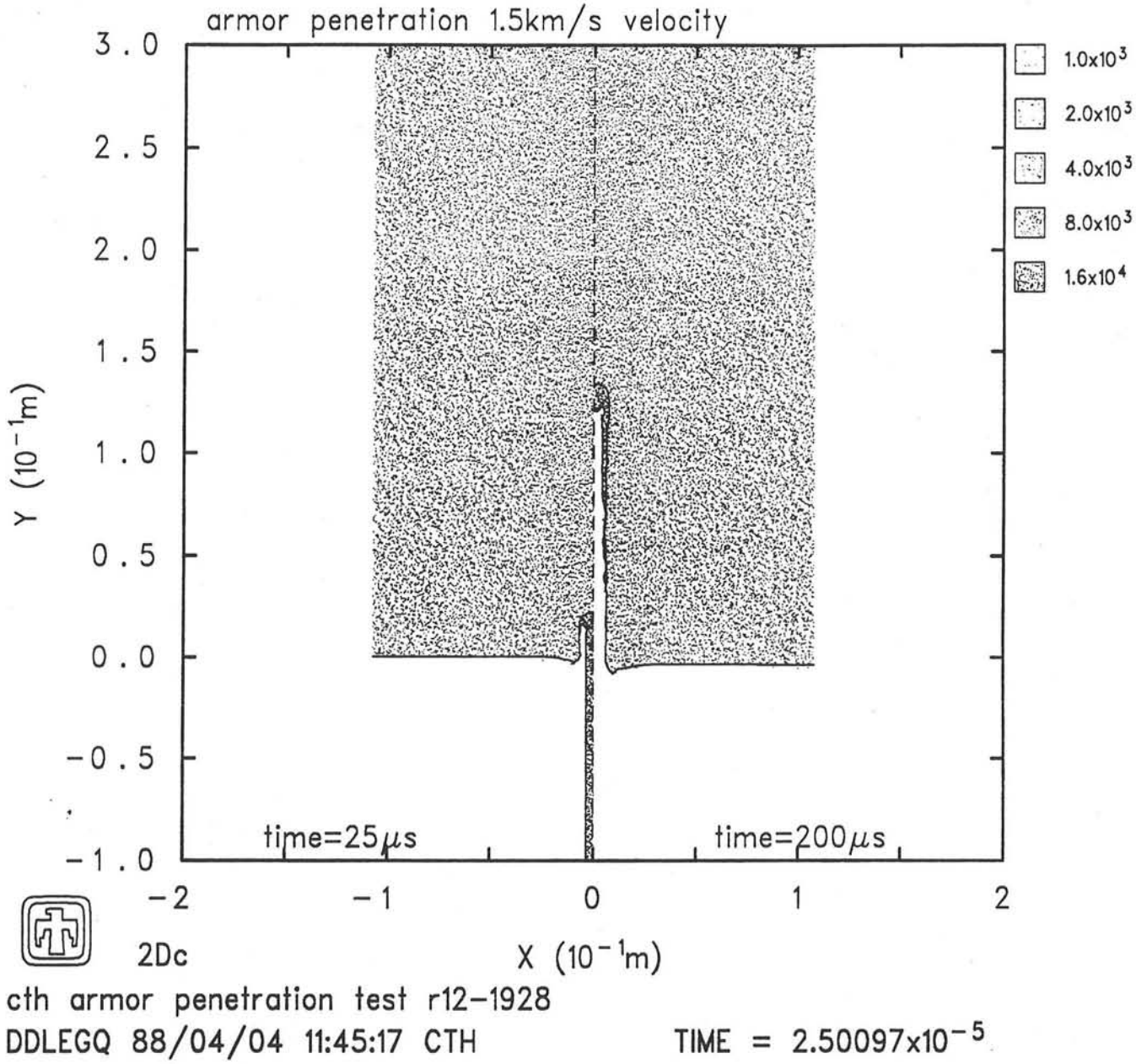

Figure 3. CTH Calculational Results for 2.7km/sec Impact Velocity

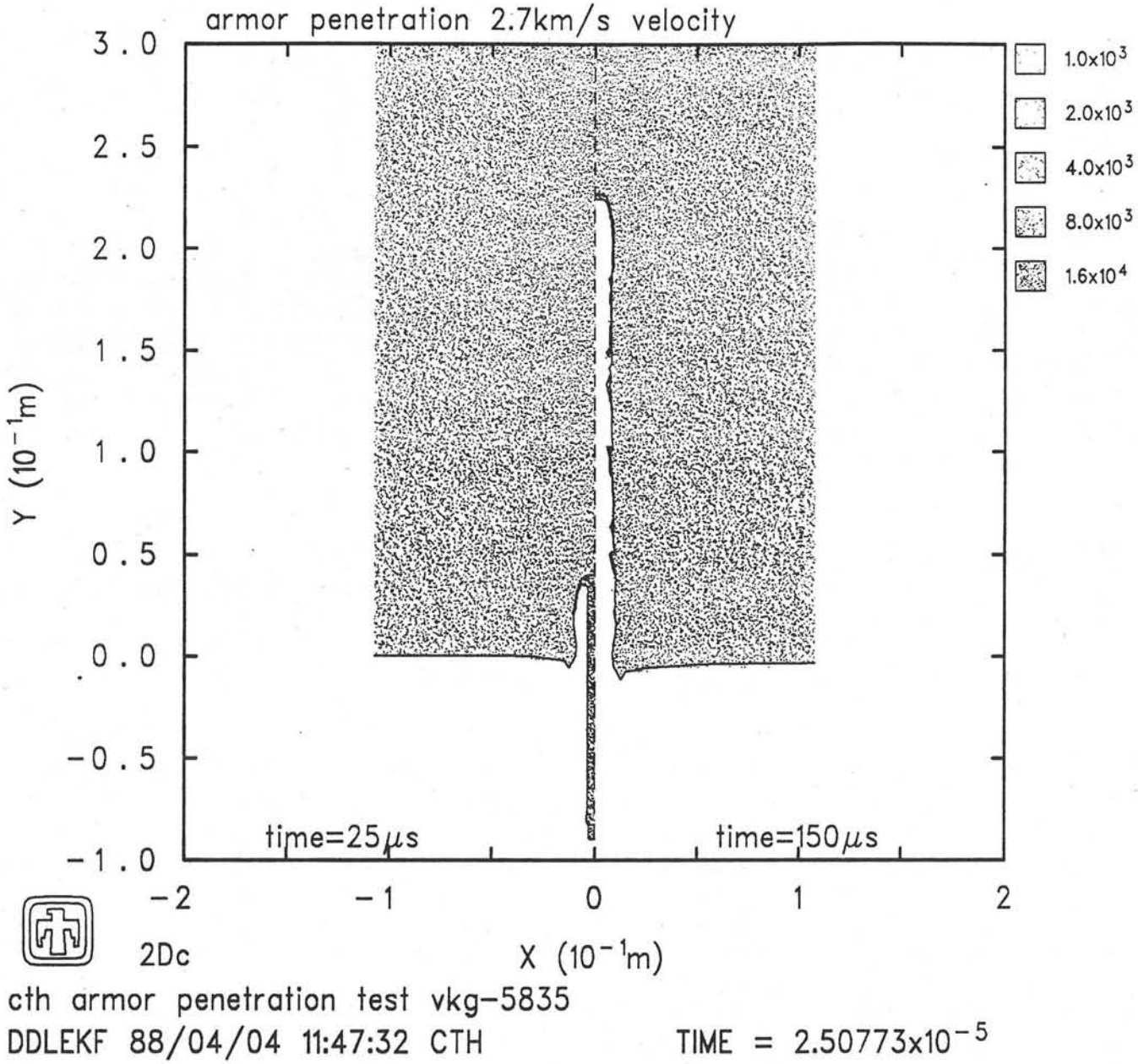

Figure 4. CTH Calculational Results for 3.3km/sec Impact Velocity

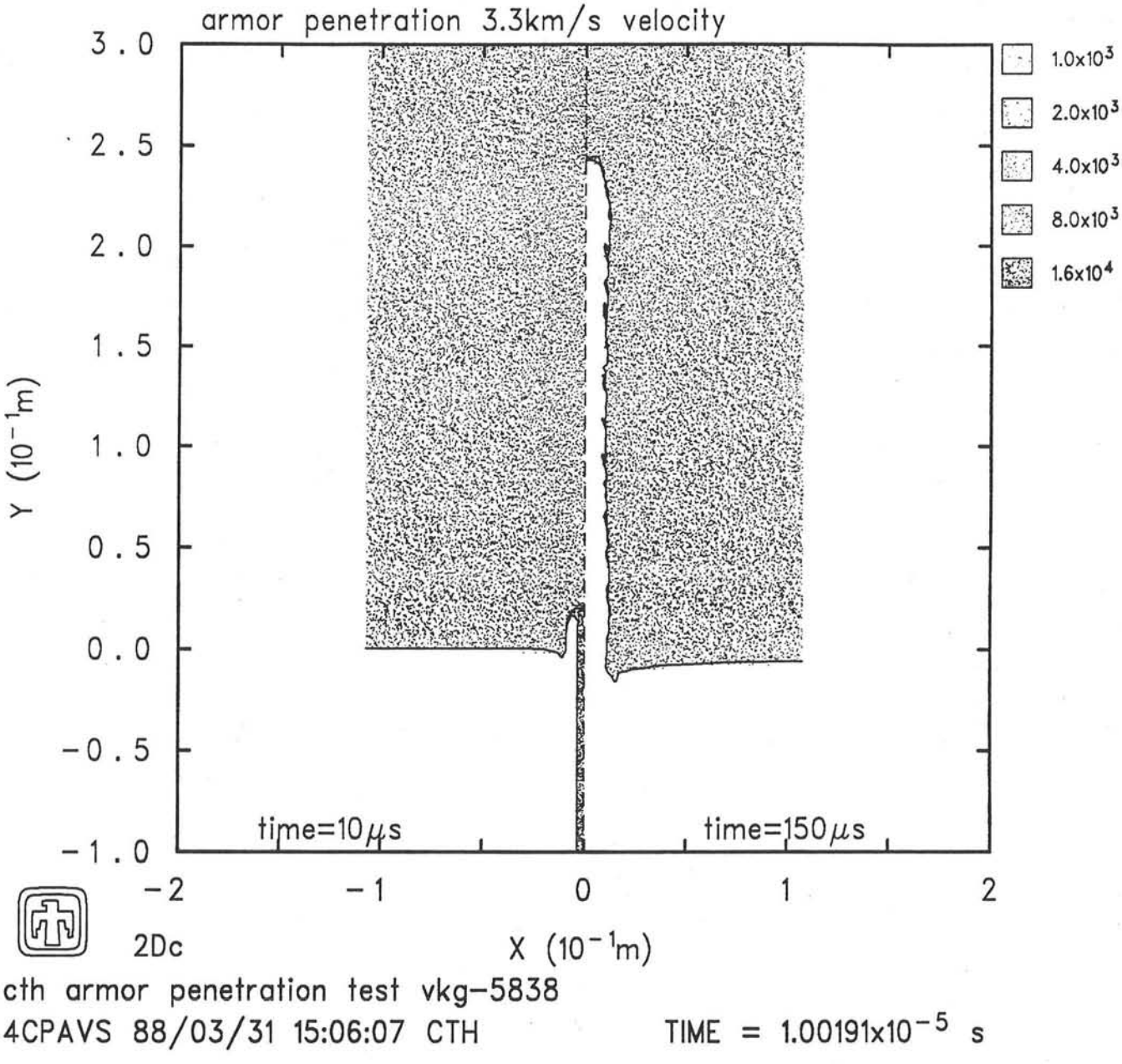

Figure 5. CTH Calculational Results for 4.4km/sec Impact Velocity

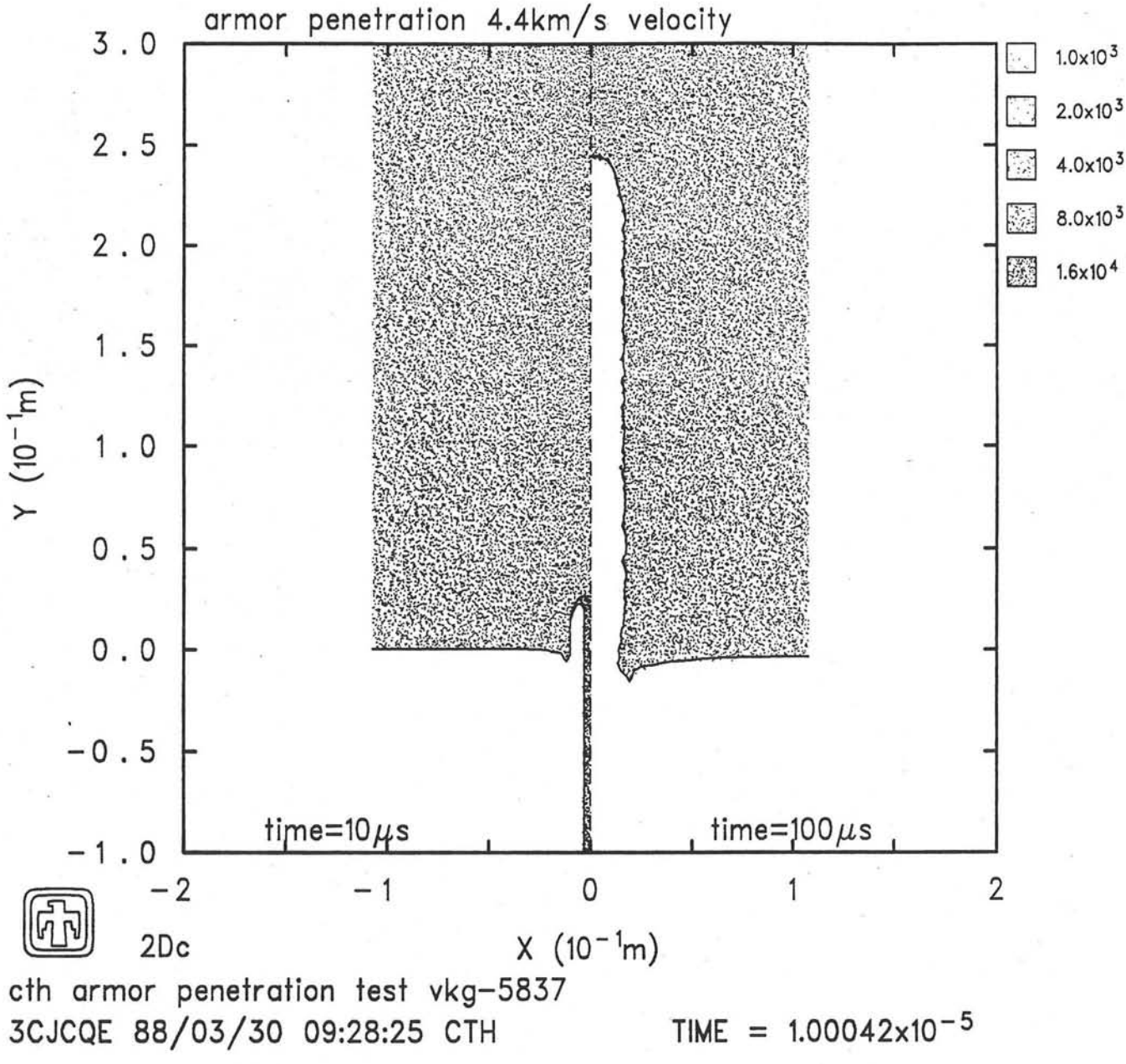

Figure 6. Comparison of CTH Results and Experimental Data for Cavity Diameter

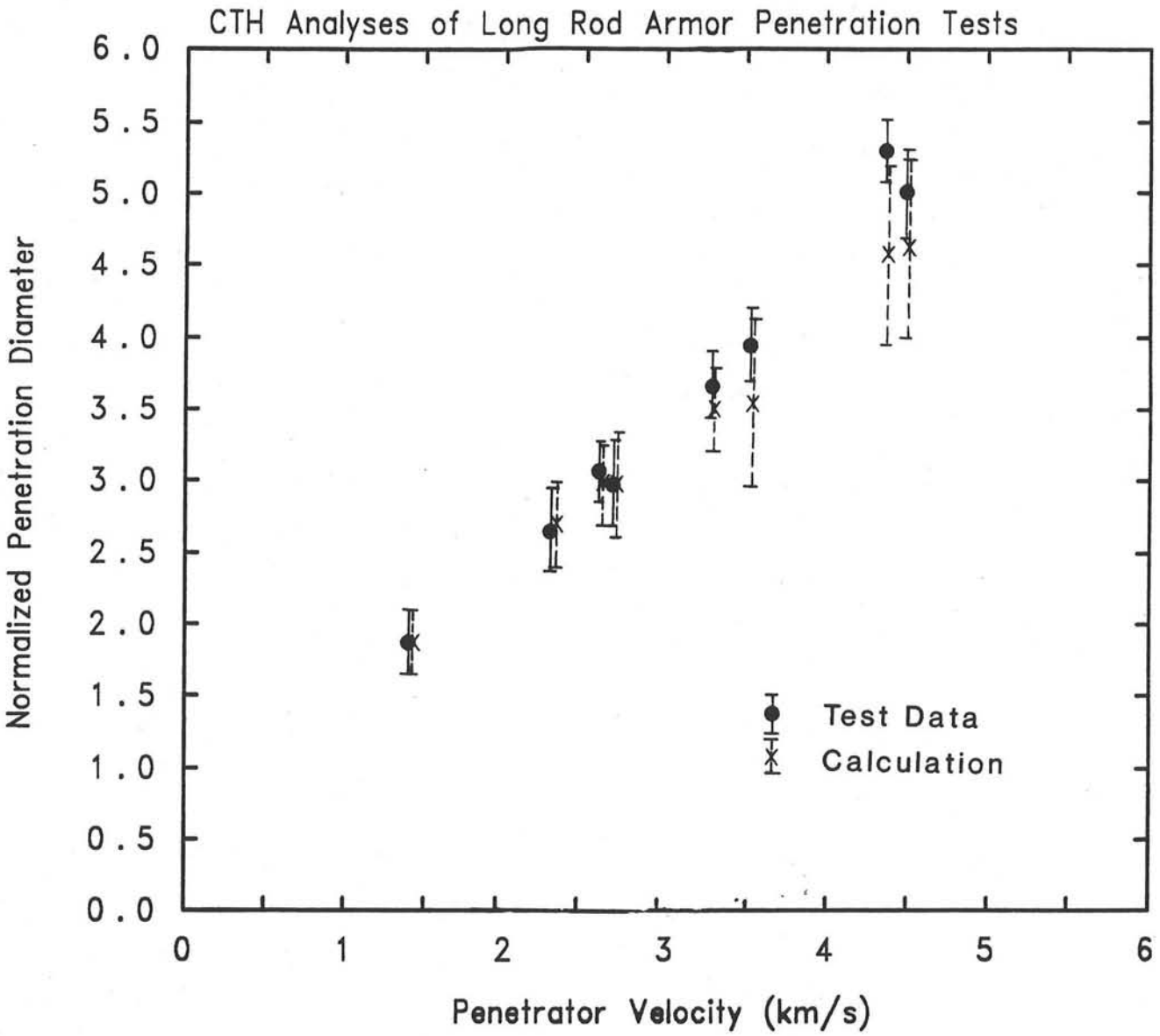

Figure 7. Comparison of CTH Results and Experimental Data for Cavity Depth

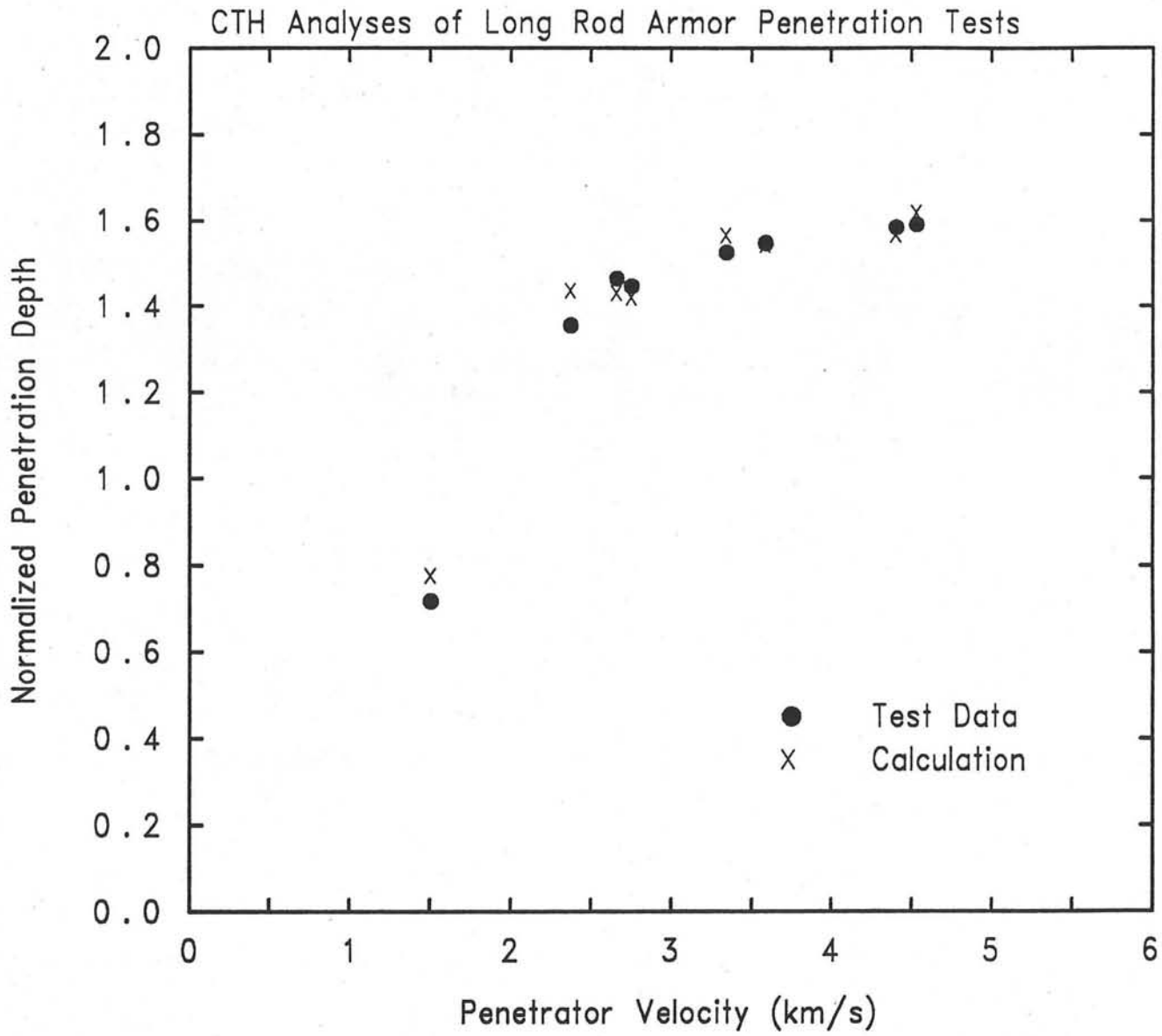

Figure 8. Comparison of Baseline and Finely-Zoned CTH Calculations for 4.4km/sec Impact Velocity

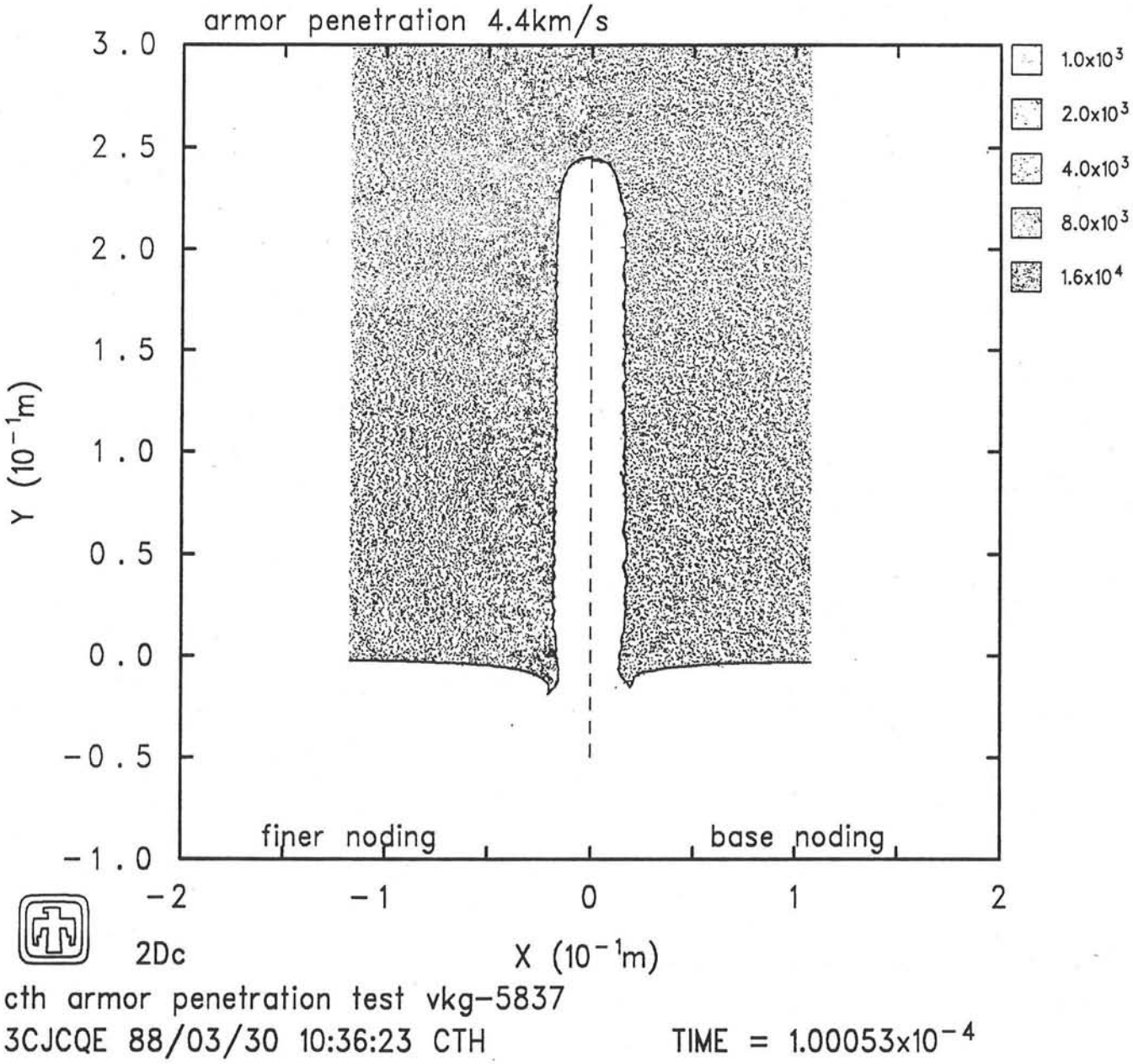

Figure 9. Results of CTH Yield Strength Sensitivity Study - Cavity Diameter for 4.4km/sec Impact Velocity

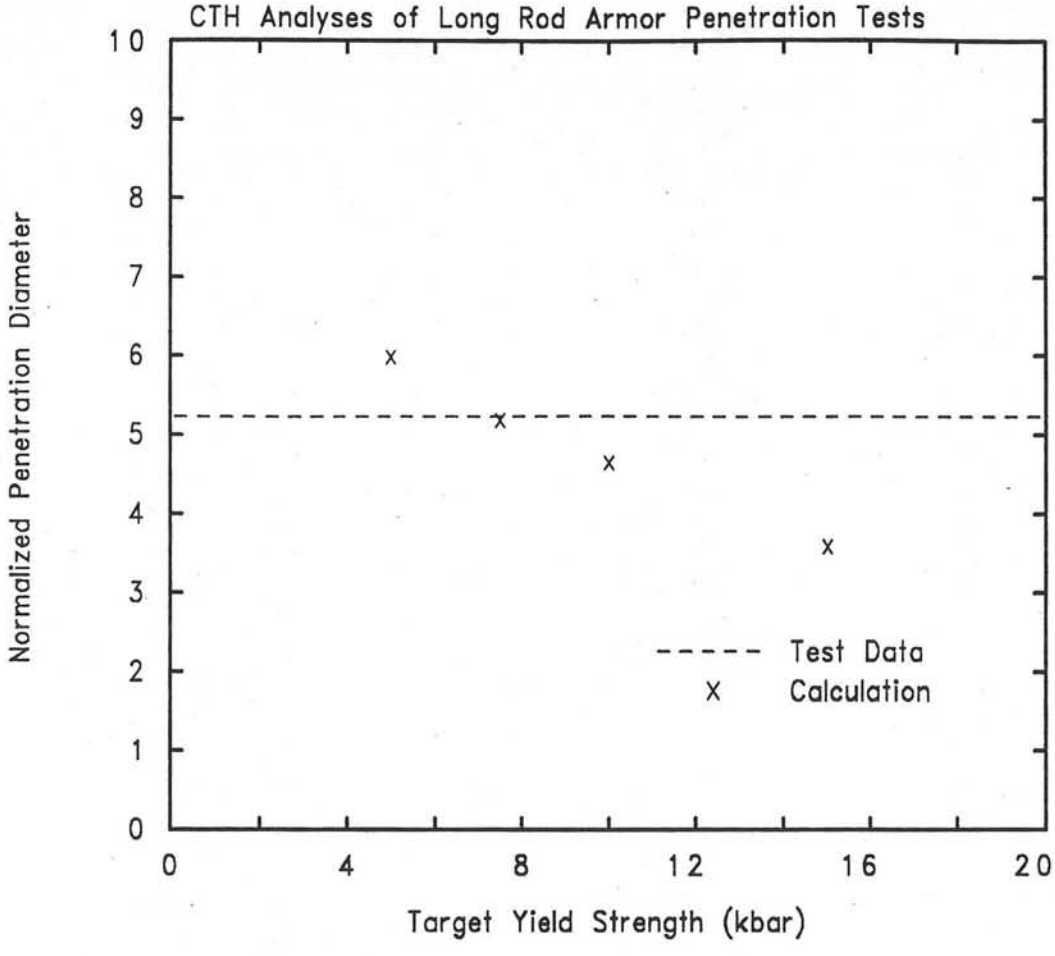

Figure 10. Results of CTH Yield Strength Sensitivity Study - Cavity Depth for 4.4km/sec Impact Velocity

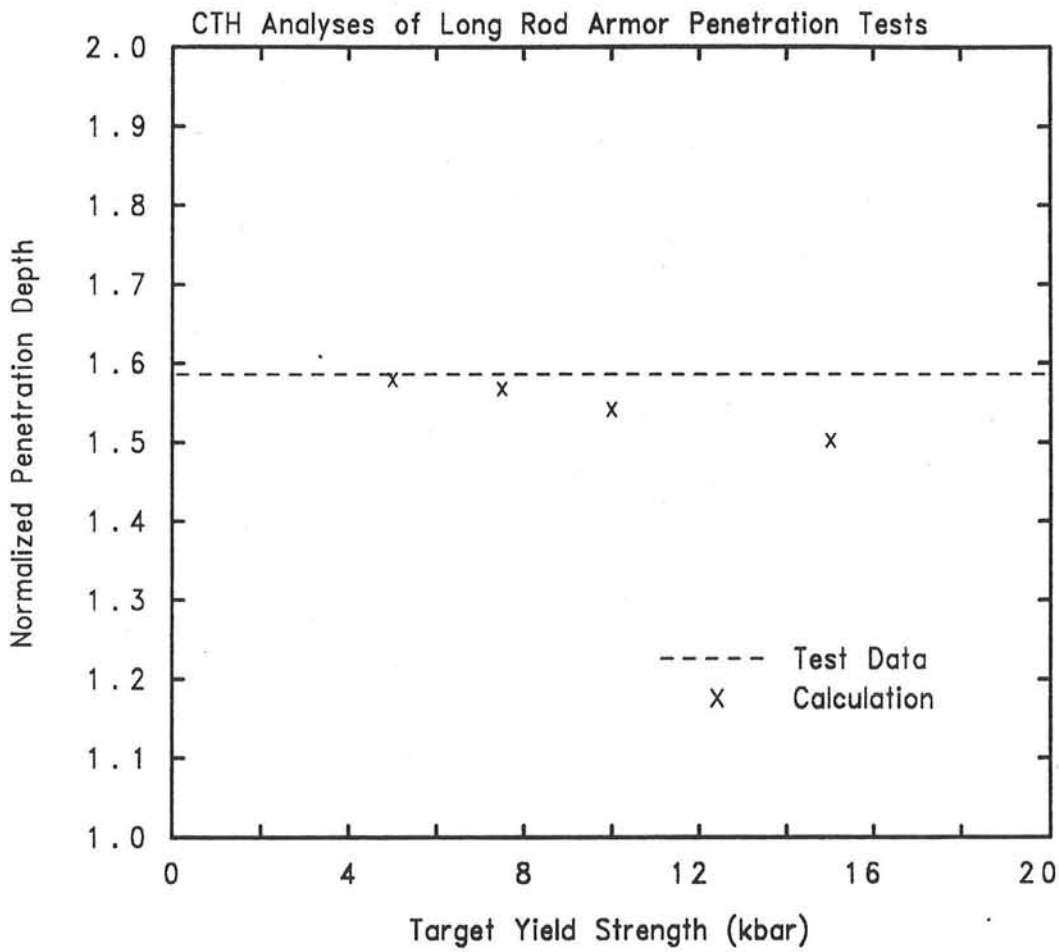

Figure 11. Comparison of 7.5kbar and 15kbar Target Strength CTH Calculations for 4.4km/sec Impact Velocity

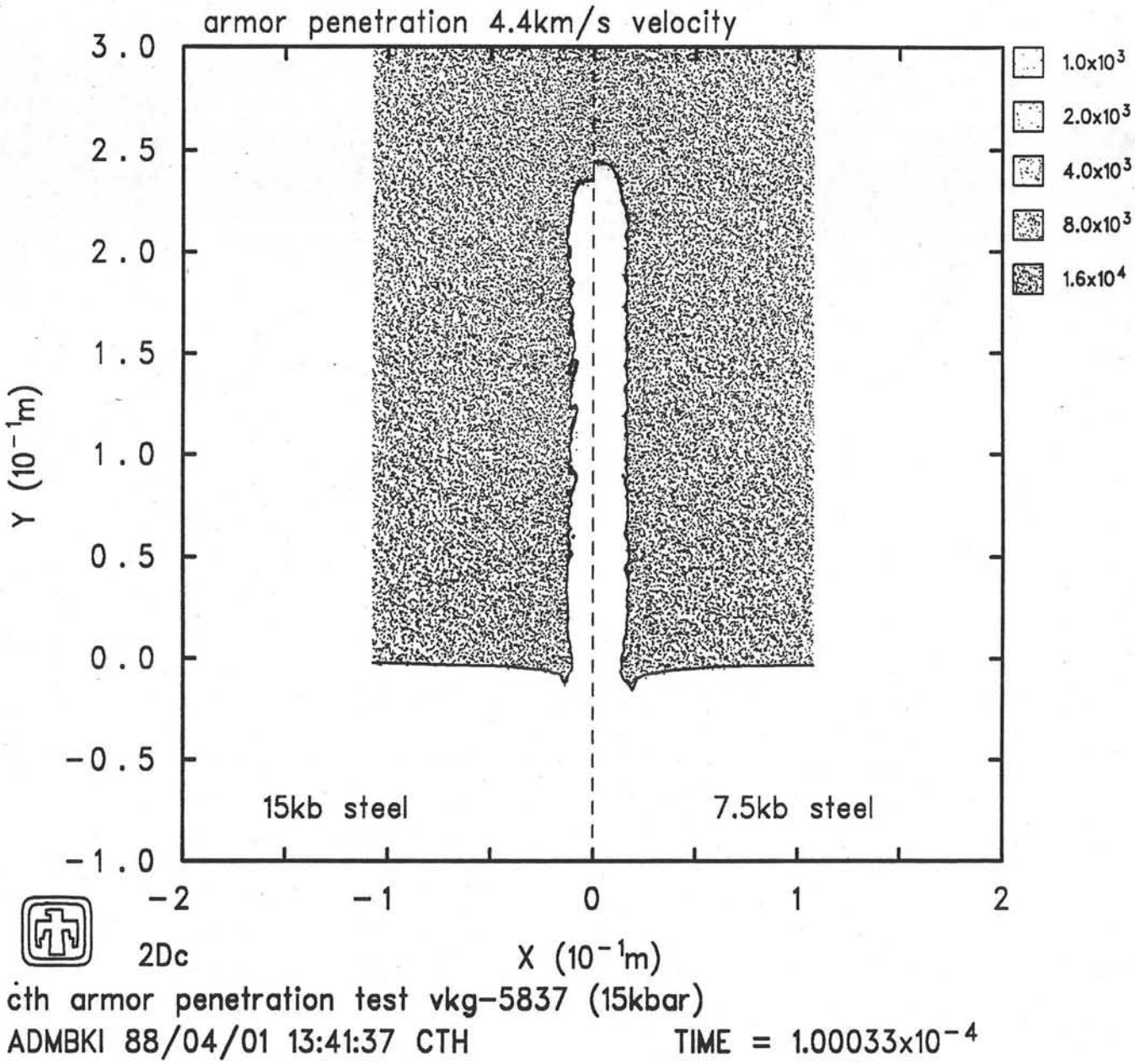

Figure 12. HULL Calculational Results for 1.5km/sec Impact Velocity

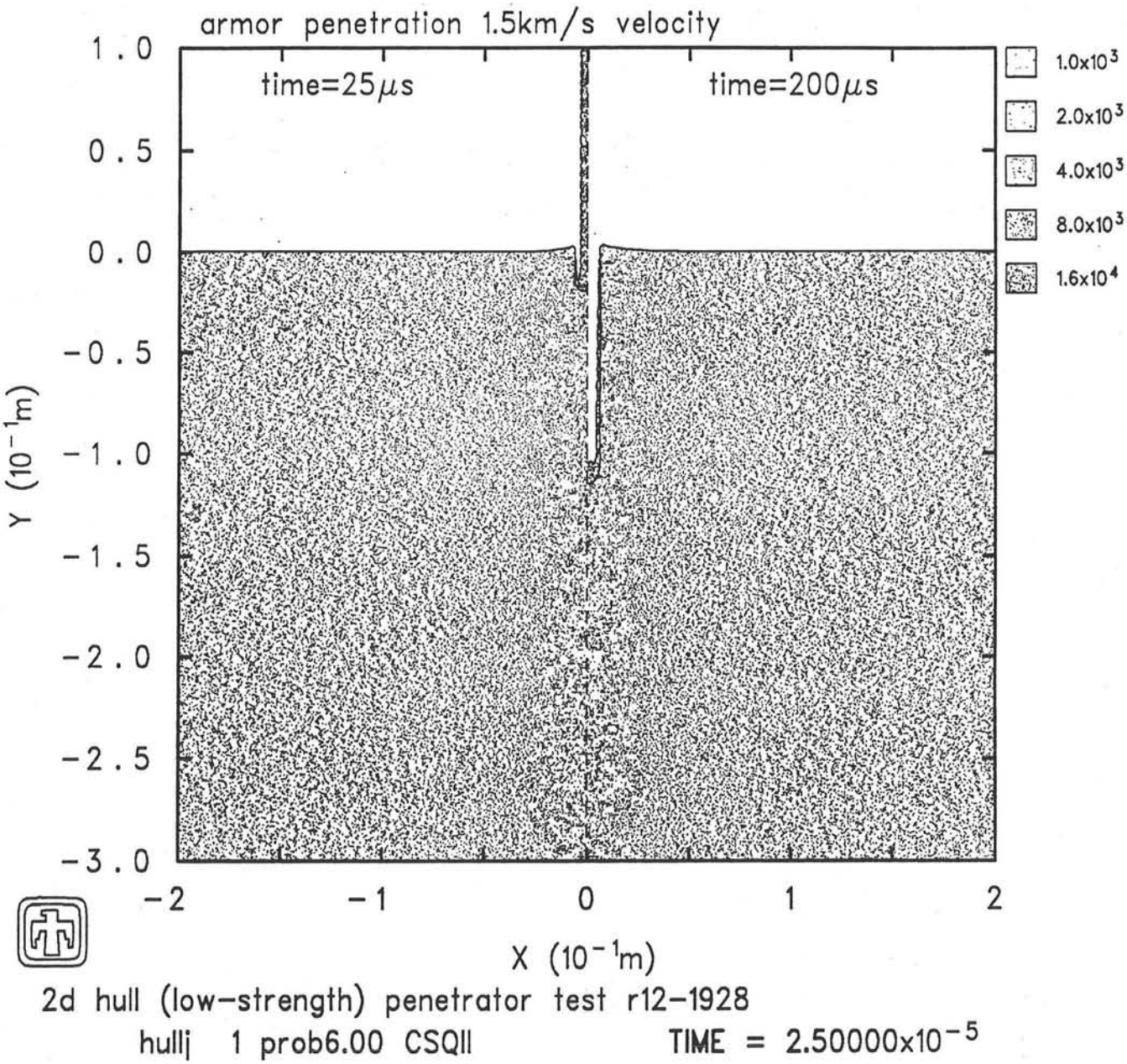

Figure 13. HULL Calculational Results for 2.7km/sec Impact Velocity

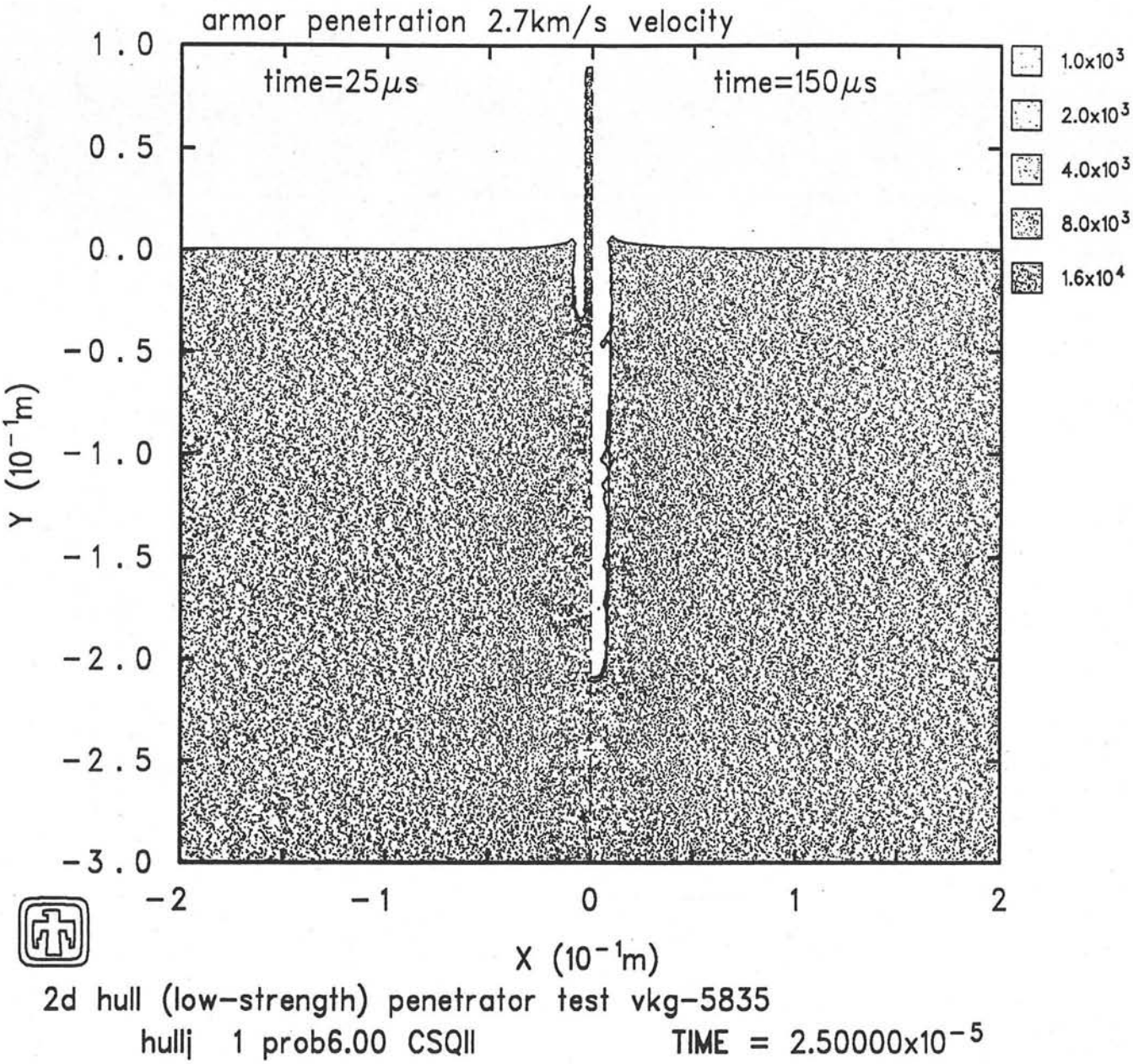

Figure 14. HULL Calculational Results for 3.3km/sec Impact Velocity

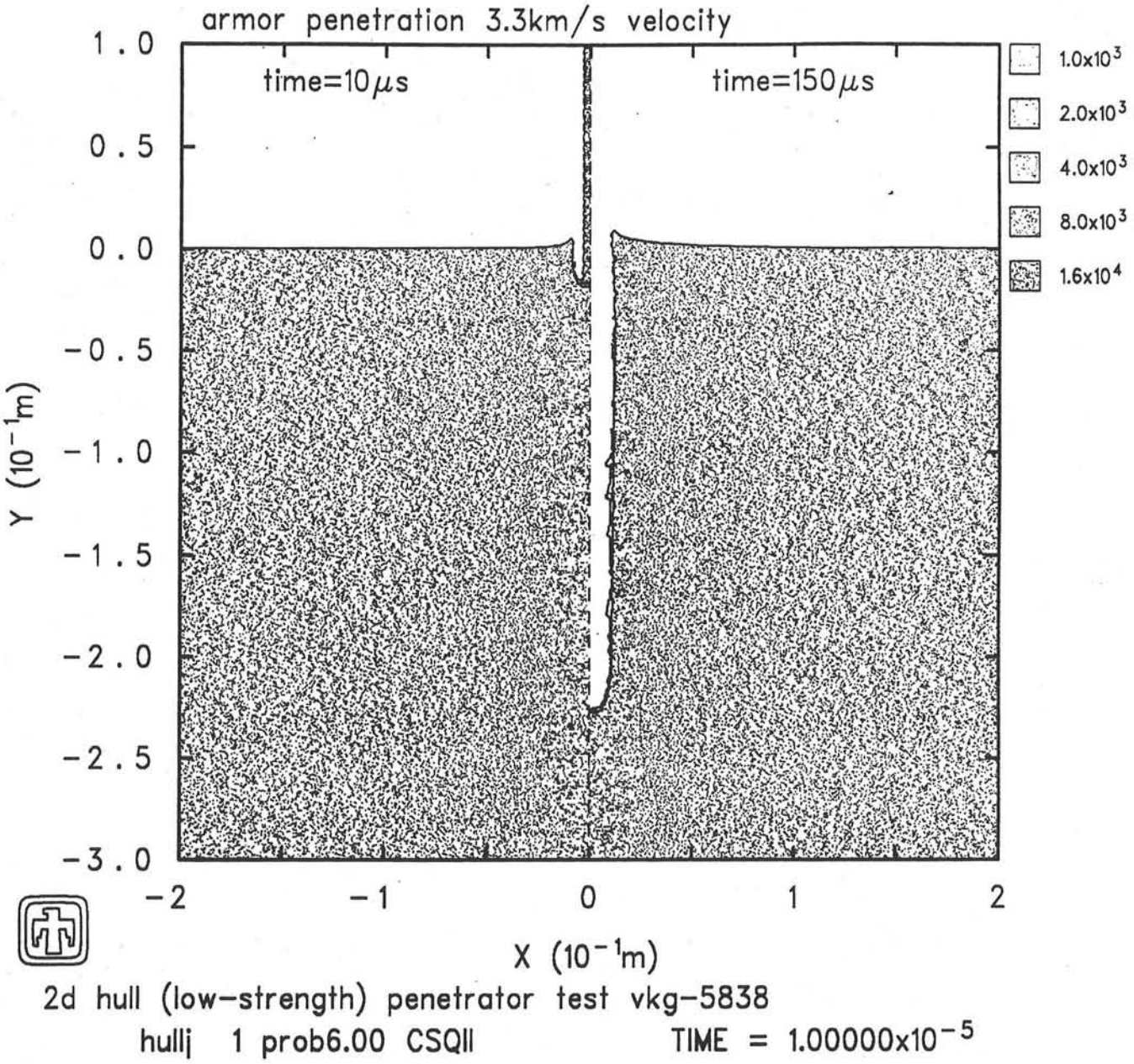

Figure 15. HULL Calculational Results for 4.4km/sec Impact Velocity

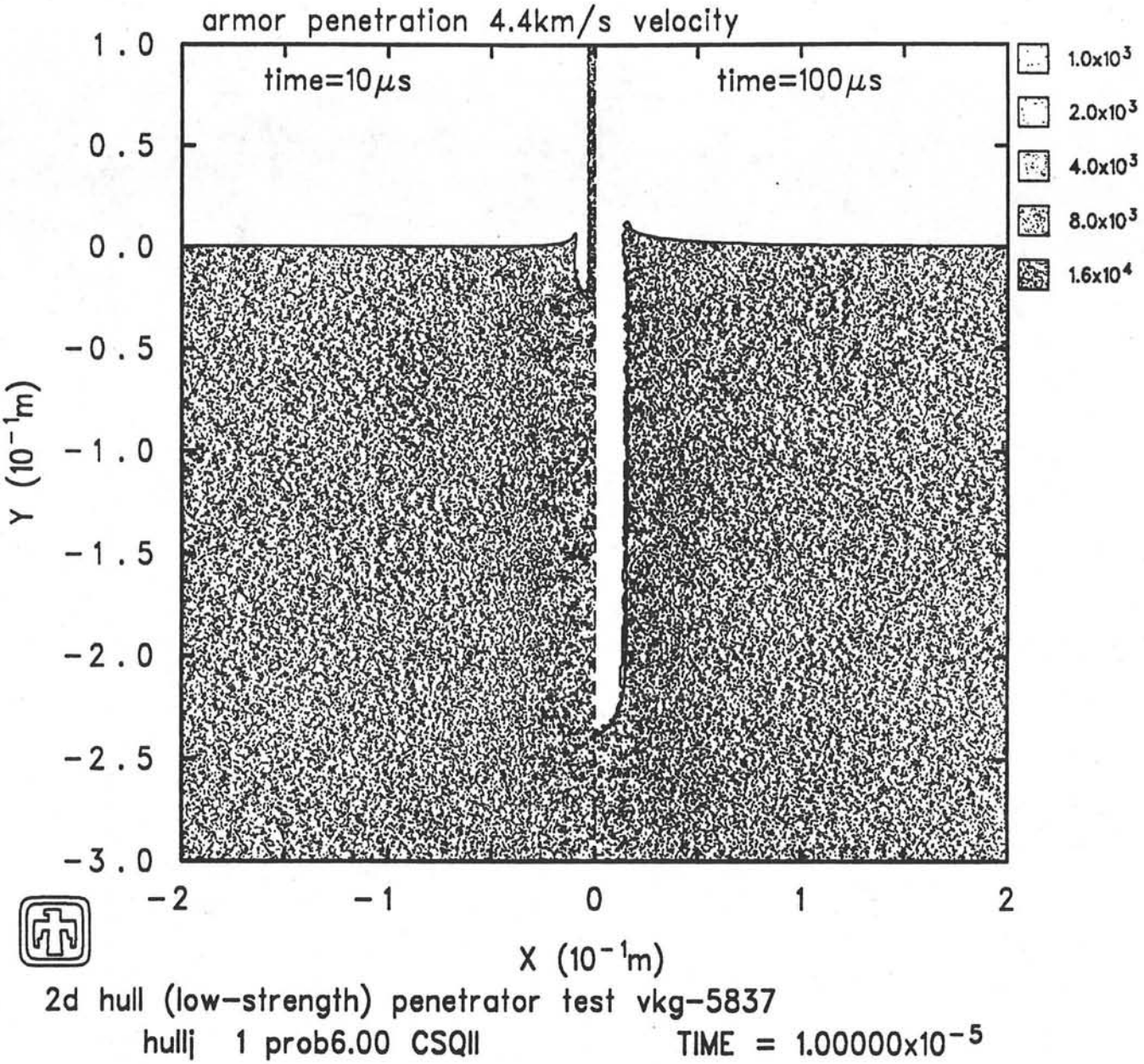

Figure 16. Comparison of HULL Results and Experimental Data for Cavity Diameter

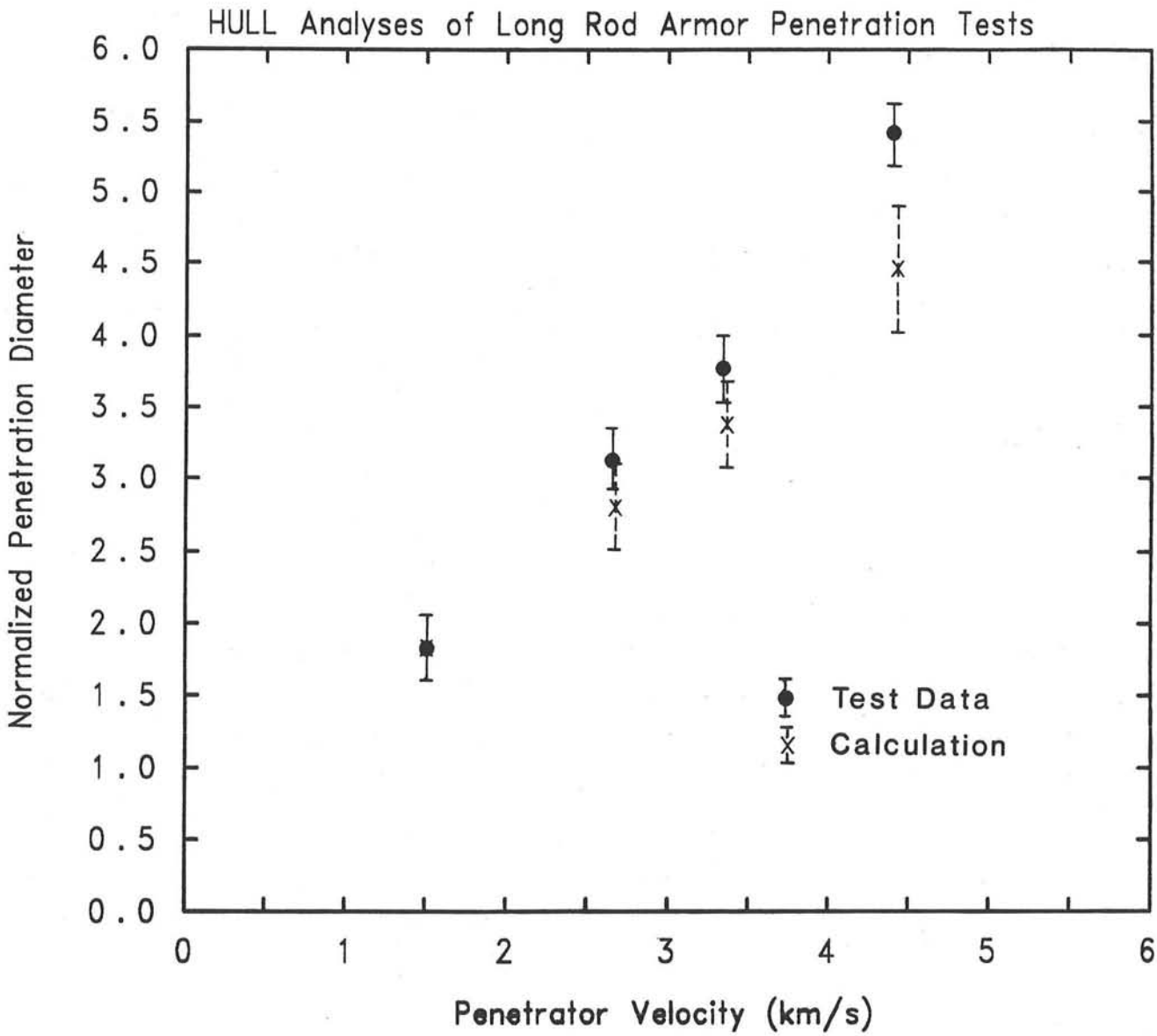

Figure 17. Comparison of HULL Results and Experimental Data for Cavity Depth

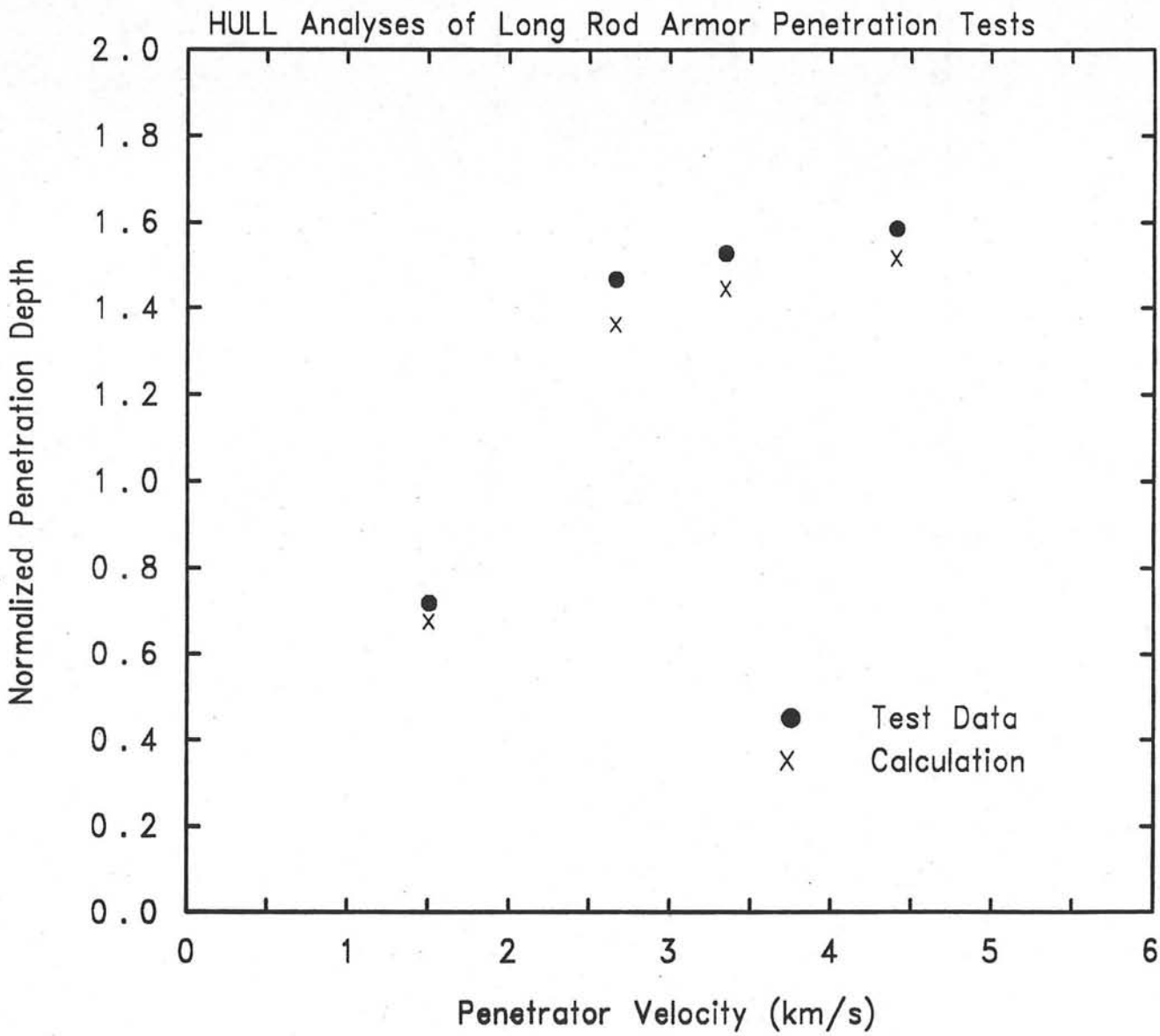

Figure 18. Comparison of 7.5kbar and 15kbar Target Strength HULL Calculations for 4.4km/sec Impact Velocity

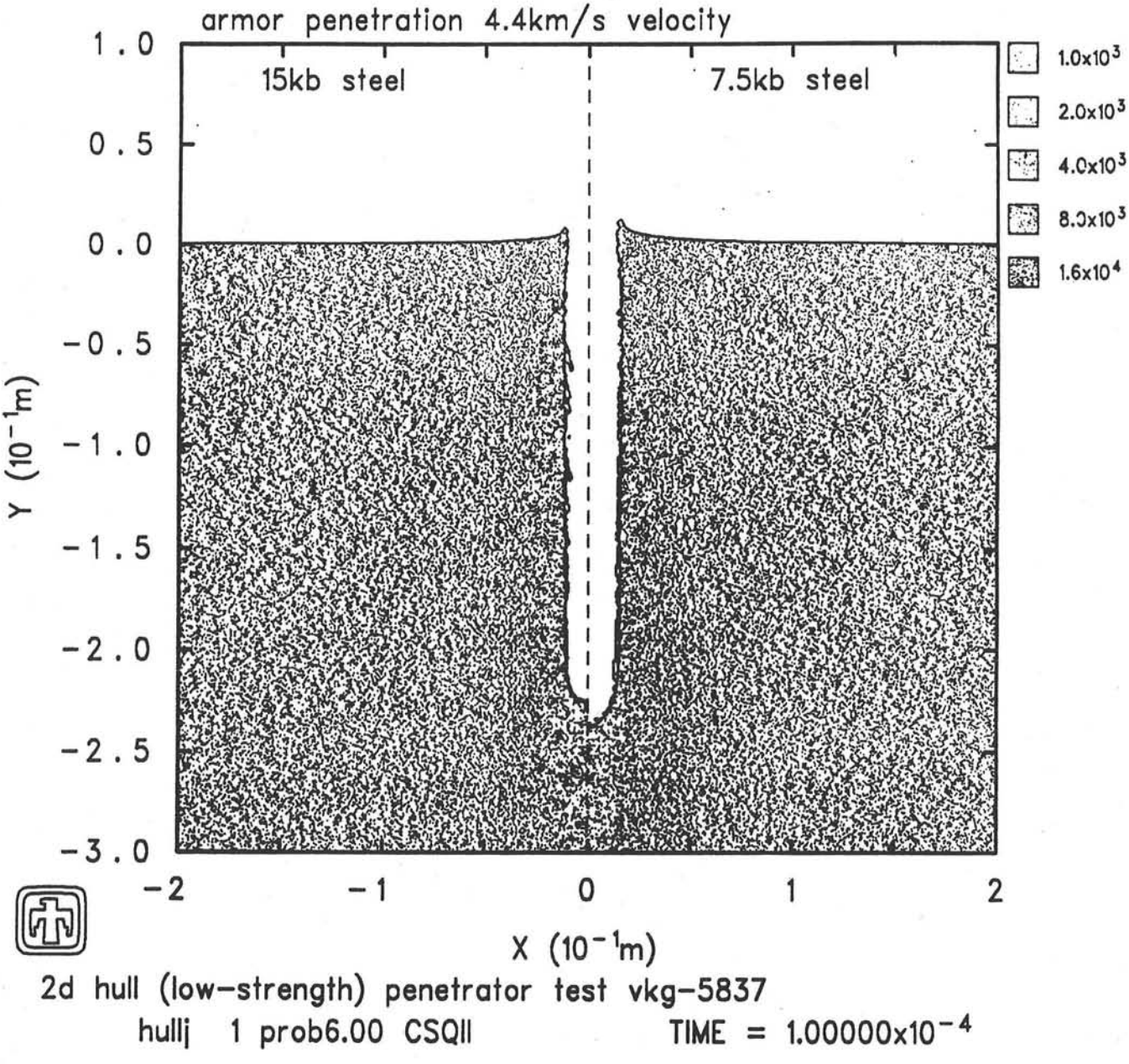

APPENDIX A. CTH Calculations

A.1 CTH Input Deck

The CTHGEN and CTH input used for the 4.4km/s (Test No. VKG-5837 [3]) basecase calculation are shown below. The CTHGEN deck shows the zoning, the material insertion packages, and the material equation-of-state properties used for the calculations. The CTH deck specifies the edit frequencies, the material strength and fracture values, and the boundary conditions for the calculation.

A.2 CTH Code Version

Most of the calculations were done with version 1.01.b <03/24/88>, without any additional code updates; one calculation was done with version 1.03.e <05/06/88> (with fracture specified on maximum principal stress rather than pressure).

A.3 CTH Output Files

A number of CTH calculations were done for this armor penetration study. The results of any given calculation are ASCII output files for the CTHGEN and CTH runs (which echo the input streams), and binary restart and plot files. All such files for the CTH armor penetration study are in the IFS directory /e00021674/cth2-armor.

Beside the files for the basecase calculations, this IFS node contains a number of subdirectories. Several input control decks can be found in the subdirectory /input-files. The other subdirectories contain the results for the following sensitivity studies:

A: /strength-study (varying the target yield strength), and

B: /finer-nodes (halving the cell size used).

The particular test being simulated in a given run is specified by the hyphenated tag end on the file name (e.g., rscth-vkg5837).

```
*
*eor*cgenin
*
cth armor penetration test vkg-5837
*
control
  ep
* mmt
* usessd
endcontrol
*
mesh
  block 1  geom 2dc  type e
    x0 0.
      x1  n 10  dxf 0.10  rat 1.0
      x2  n 50  dxf 0.10  rat 1.025
    endx
    y0 -20.0
      y1  n 250  dyf 0.20  w 50.0
      y2  n 50  dyf 0.20  rat 1.05
    endy
    xact 0.0 1.0
    yact -20.0 1.0
  endblock
endmesh
*
material insertion
  block 1
    package 'target'
      material 1
      numsub 25
      insert box
        x1 0.0  x2 1000.0
        y1 0.0  y2 1000.0
      endinsert
    endpackage
    package 'rod'
      material 2
      numsub 25
      velocities yvel 4.398e5
      insert box
        x1 0.0  x2 0.3345
        y1 -15.575  y2 0.0
      endinsert
    endpackage
  endblock
endinsertion
*
edit
  block 1
    expanded
  endblock
endedit
*
eos  num 2
  mat1 -1
  mat2 -2
    aneos  -1  iron  lib=5  type=3
    aneos1  -2  tungsten  rhug=-1  thug=-1
    aneos2  1.  4.  19.30  0.  0.  -4.03e5  1.54  -.036
    aneos3  1.237  2.  4.52e10  .315  0.0  0.0  0.0  0.
    aneos4  0.0  0  0  0  0  0  1.925e9  0.0
    aneos5  74.  1.
endeos
```

```
*
endinput
*
*eor*cthin
*
cth armor penetration test vkg-5837
*
control
  tstop 1.0e-04
  cpshift 999.
* pvoid 10.0
* usessd
endcontrol
*
edit
  shortt
    time 0.  dtfrequency 1.0e-06
  ends
  longt
    time 0.  dtfrequency 1.0e-05
    expanded
  endl
  plott
    time 0.  dtfrequency 1.0e-05
  endp
  histt
    time 0.  dtfrequency 1.0e-06
  endh
ende
*
boundary
  bhydro
    block 1
      bxbot 0
      bxtop 1
      bybot 1
      bytop 1
    endb
  endh
endb
*
epdata
  matep 1  yield 7.5e9  poisson 0.33
  matep 2  yield 10.0e9  poisson 0.30
  mix 2
ende
*
fracts
  pressure
    pfmix -1.0e6
    pfvoid -1.0e6
    pfrac1 -20.0e9
    pfrac2 -30.0e9
endf
*
```

APPENDIX B. HULL Calculations

B.1 HULL Input Deck

The KEEL and HULL input used for the 1.5km/s (Test No. R12-1928 [3]) basecase calculation are given below. The KEEL deck shows the zoning used and the material insertion packages. The HULL deck specifies the edit frequencies, the automatic rezone options and values, and the boundary conditions for the problem. Default material properties were modified in MATLIB, and a listing of the KEEL output showing the actual values used in the calculations is also provided.

B.2 HULL Code Version

Most of the calculations were done with HULL version 120, with change (update) decks as shown in the following SAIL input listing. Some of the change decks have been provided for HULL version 120 by Orlando Technologies, Inc., principal sponsoring organization for the HULL code system. These change decks are documented on the log files stored as part of the standard SNLA archive procedure for calculation results.

B.3 HULL Output Files

The results of any given calculation include ASCII output files for the KEEL and HULL runs (which echo the input streams), binary restart and plot files, and a RUN-HULL procedure (CTSS) log file. All such files for the HULL armor penetration study are in the IFS directory /e00021674/hull2-armor.

This IFS node contains a number of subdirectories. Several input control decks can be found in the subdirectory /input-files. The other subdirectories contain the results for the following calculations:

A: /low-strength (initial calculations),

B: /high-strength (increased target strength), and

C: /bigger-mesh (final basecase calculations).

The particular test being simulated in a given run is specified by the hyphenated tag end on the file name (e.g., hul44a-vkg5837).

```
*eor*keelin
keel  prob 6.0
 dimen 2  imax 200  jmax 550  stress 1  fail 1  strain 1  dvisc 1
  iq 10  jq 550
 nm 4  air 1  w10 2  ssteel 3  rha 4
   ygnd -1.e20
 nop 0 nstn 0   header
  2d hull (low-strength) penetrator test r12-1928
mesh
 constant subgrid
         x0lim 0.  x0 0.  nx 10  dx 0.05  xmax 0.5  rxpos 1.05
         y0  -34.00  ny 500  dy 0.10  ymax 16.00  ymlim 16.00
generate
 package  air  rectangle  y0 0.
   delete rectangle  y0 0.  y2 15.583  x0 0.  x2 0.3410
 package  w10  v -1.494e5  rectangle  y0 0.  y2 15.583  x0 0.  x2 0.3410
 package  ssteel  rectangle  y0 -1000.0  y2 0.
end
*eor*hullin
hull prob 6.0
cycle 9999
 input
 times 3 dmpint .000025
  ptstop .000250 mreler 2.e4
   visc 1  dvisc 2  stabf .5  rezone 0
  ygnd -1.e20
  expand .05
  nstn 0  nop 0
*eor*sailin
sail liheno  options
inst 14  cray 1  sys 1  ctss 1  sensesw 1
mmap=0
nhilr=0
endoptions
*read ch120a
*read chctss
*read ch120
*read ch6418
*read chrez
```

```
material property data for material named air
            ambient density =  1.2250e-03
        ambient sound speed =  3.4029e+04
             ambient energy =  2.0679e+09
                      gamma =  1.4000e+00
units are assumed to be cgs

material property data for material named w10
             ambient density =  1.7300e+01
         ambient sound speed =  4.0000e+05
shock vel/particle vel slope =  1.2680e+00
             gruneisen ratio =  1.5800e+00
            minimum pressure = -4.0000e+09
              poissons ratio =  3.0000e-01
            rigidity modulus =  1.2775e+12
               atomic weight =  0.1840e+03
           debye temperature =  0.2700e+03
     vapor state coefficient =  0.2000e+00
              ambient energy =  0.2626e+09
         ambient melt energy =  0.4770e+10
               fusion energy =  0.1840e+10
          sublimation energy =  0.4600e+11
energy at beginning of vapor =  0.1360e+11
      energy at end of vapor =  0.5840e+11
      initial yield strength =  1.1650e+10
      maximum yield strength =  1.1850e+10
     strain at maximum yield =  1.0600e-01
thermal softening coeff   yf1 =  9.0000e-01
thermal softening coeff   ef1 =  5.0000e-01
thermal softening coeff   yf2 =  9.0000e-01
thermal softening coeff   ef2 =  5.0000e-01
  principal stress at failure =  0.1000e+51
  principal strain at failure =  0.1000e+51
units are assumed to be cgs

material property data for material named ssteel
             ambient density =  7.8600e+00
         ambient sound speed =  4.6100e+05
shock vel/particle vel slope =  1.7300e+00
             gruneisen ratio =  1.6700e+00
            minimum pressure = -1.0000e+20
              poissons ratio =  3.0930e-01
            rigidity modulus =  7.2989e+11
               atomic weight =  0.5585e+02
           debye temperature =  0.3550e+03
     vapor state coefficient =  0.2500e+00
              ambient energy =  0.7556e+09
         ambient melt energy =  0.7400e+10
               fusion energy =  0.2740e+10
          sublimation energy =  0.7420e+11
energy at beginning of vapor =  0.2240e+11
      energy at end of vapor =  0.8680e+11
      initial yield strength =  7.5000e+09
      maximum yield strength =  7.5000e+09
     strain at maximum yield =  1.5000e-01
thermal softening coeff   yf1 =  9.0000e-01
thermal softening coeff   ef1 =  5.0000e-01
thermal softening coeff   yf2 =  9.0000e-01
thermal softening coeff   ef2 =  5.0000e-01
```

```
 principal stress at failure =  0.6000e+11
 principal strain at failure =  0.3000e+00
units are assumed to be cgs

material property data for material named rha
                ambient density =  7.8600e+00
            ambient sound speed =  4.6100e+05
shock vel/particle vel slope =  1.7300e+00
               gruneisen ratio =  1.6700e+00
              minimum pressure = -1.0000e+20
                poissons ratio =  2.6000e-01
              rigidity modulus =  9.5452e+11
                 atomic weight =  0.5585e+02
             debye temperature =  0.3550e+03
      vapor state coefficient =  0.2500e+00
                ambient energy =  0.7556e+09
           ambient melt energy =  0.7400e+10
                 fusion energy =  0.2740e+10
            sublimation energy =  0.7420e+11
energy at beginning of vapor =  0.2240e+11
        energy at end of vapor =  0.8680e+11
       initial yield strength =  1.5000e+10
       maximum yield strength =  1.5000e+10
      strain at maximum yield =  3.0000e-01
thermal softening coeff   yf1 =  9.0000e-01
thermal softening coeff   ef1 =  5.0000e-01
thermal softening coeff   yf2 =  9.0000e-01
thermal softening coeff   ef2 =  5.0000e-01
  principal stress at failure =  0.4200e+11
  principal strain at failure =  0.1750e+01
    number of (p/y,ep) points =          7
       p/y          ep
 -1.5000e+00   5.0000e-02
 -1.3000e+00   1.3000e-01
 -8.0000e-01   2.0000e-01
 -5.0000e-01   5.0000e-01
 -3.0000e-01   1.0000e+00
 -1.0000e-01   2.0000e+00
  2.0000e-01   5.0000e+00
```

EXTERNAL DISTRIBUTION:

Alcoa Laboratories (2)
ATTN: R. Young
J. McMichael
Aluminum Company of America
Alcoa Center, PA 15069

Army Material Technology Laboratory
SLCMT-MRD
ATTN: K. Ofstedahl
Arsenal Street
Watertown, MA 02172

Orlando Technology, Inc.
ATTN: D. Matuska
Box 855
Shalimar, FL 32579

Department of the Army
U.S. Army Laboratory Command
Ballistic Research Laboratory (3)
ATTN: G. Silsby
K. Kimsey
G. Randers-Pehrson
Aberdeen Proving Ground, MD 21005-5066

Los Alamos National Laboratory (4)
ATTN: G. Cort, WX-4
M. Burkett, WX-4
D. Mandell, X-7
N. Johnson, T-3
P. O. Box 1663
Los Alamos, NM 87545

INTERNAL DISTRIBUTION:

1500 W. Herrmann
1510 J. W. Nunziato
1520 L. W. Davison
1524 A. K. Miller
1530 D. B. Hayes
1531 S. L. Thompson
1531 L. N. Kmetyk (20)
1531 J. M. McGlaun
1531 J. S. Rottler
1531 J. W. Swegle
1533 P. Yarrington (20)
1533 W. T. Brown
1533 G. I. Kerley
1533 M. E. Kipp
1533 S. T. Montgomery
1533 F. R. Norwood
1533 A. C. Robinson
1534 J. R. Asay
1534 D. E. Grady
1534 T. G. Trucano
1534 J. L. Wise
1550 C. W. Peterson
3141 S. A. Landenberger (5)
3141-1 C. L. Ward (8) for DOE/OSTI
3151 W. I. Klein (3)
8524 J. A. Wackerly
9014 R. J. Lawrence
9120 M. M. Newsom
9122 R. H. Braasch
9122 M. J. Forrestal
9122 V. K. Luk
9122 R. O. Nellums
9130 R. D. Andreas